Soft Matter

PAPER

View Article Online
View Journal | View Issue

Cite this: *Soft Matter*, 2018, **14**, 6119

Relaxation dynamics of saturated and unsaturated oriented lipid bilayers†

Hirsh Nanda,‡[a] Victoria García Sakai,[b] Sheila Khodadadi,§[a] Madhu Sudan Tyagi,[ac] Edwin J. Schwalbach ¶[d] and Joseph E. Curtis *[a]

Received 25th August 2017,
Accepted 19th June 2018

DOI: 10.1039/c7sm01720k

rsc.li/soft-matter-journal

We present experimental measurements and analysis of the dynamics and the phase behaviour of saturated DMPC and unsaturated DOPC oriented multi-lamellar bilayers. Elastic and inelastic neutron scattering were used to directly probe the dynamical processes of these membrane systems on time and length scales relevant to the internal and localized motion of lipid monomers. Mobility in this regime can be informative in elucidating the local interactions responsible for material properties of these fluid lipid systems. DMPC and DOPC are structurally similar in terms of their membrane hydrophobic thickness; however, they exhibit different mechanical properties in terms of both elastic compressibility and bending moduli. The analyses suggest that the constraint imposed by the double bonds in DOPC acyl chains restricts atomic motion in both liquid and gel phases compared to DMPC. We discuss applications of molecular dynamics to further elucidate the atomic details of the dynamical processes. Such an understanding may suggest how membrane properties can be tuned using a variety of different lipid species.

Introduction

The dynamics of biological membranes are important for many processes including the transport of small molecules, gating and function of transmembrane proteins and the architectural re-shaping of membranes for example in vesiculation or cell motility. For many of these processes, flexibility and membrane fluidity play a key role, and how they are affected by lipid composition and type, hydration and temperature conditions. Our conceptual view of lipid membranes is largely that of two-dimensional fluids with lipids and proteins diffusing within the membrane planes.[1] The individual lipid monomers that compose biological membranes are chemically heterogeneous and themselves have many internal degrees of freedom. As a result, biological membranes exhibit complex molecular dynamics over a range of time and length scales from picoseconds to seconds and from Angstroms to microns. More recently, our understanding of non-ideal mixing in multi-lipid systems has suggested the co-existence of laterally separated domains that may themselves exhibit different dynamical behaviour, likely influencing the function of embedded proteins.[2]

Multiple relaxation processes inherent in lipid systems makes a detailed characterization of the underlying molecular mechanisms difficult. Despite extensive work in studying the dynamics of a number of lipid systems, many challenges remain. A number of experimental methods sensitive to different time scales and molecular components have been used to study model membranes. Long time scale processes such as lateral lipid diffusion and lipid "flip-flop" from one leaflet to the other can take minutes to hours and has been probed by fluorescence.[3,4] Nuclear magnetic resonance can be used to measure both collective excitation and individual lipid molecule or chain segment diffusion[5] as well as water dynamics.[6] Neutron spin-echo and dynamic light scattering are used to measure collective undulations.[7–11] Spectroscopic and scattering techniques such as dielectric spectroscopy,[12] FTIR,[13] quasielastic neutron scattering (QENS) capture localized motions (*e.g.* vibrations, rotations and diffusion).[14–23]

Neutron scattering can provide both correlation times and geometry of dynamic motions. Previous investigations have applied QENS to look in detail at the behaviour of saturated lipids in oriented multi-lamellar stacks,[6,8–10,14–20] separating in-plane and out-of-plane diffusive motions of lipid species, as

[a] *NIST Center for Neutron Research, National Institute of Standards and Technology, 100 Bureau Drive, Mail Stop 6102, Gaithersburg, MD 20899, USA. E-mail: joseph.curJs@nist.gov*
[b] *ISIS Pulsed Neutron & Muon Source, Rutherford Appleton Laboratory, Chilton, Didcot OX11 0QX, UK*
[c] *Department of Materials Science, University of Maryland, College Park, Maryland 20742, USA*
[d] *Materials Science and Engineering Department, Northwestern University, 2220 Campus Drive, Evanston, IL 60208, USA*
† Electronic supplementary information (ESI) available. See DOI: 10.1039/c7sm01720k
‡ Present address: Pharmaceutical Development and Manufacturing Sciences, Jannsen, Inc., 1400 McKean Road, Spring House, PA 19477, USA.
§ Present Address: Department of Chemical Engineering, Delft University of Technology, Netherlands.
¶ Present address: Air Force Research Laboratory, Materials and Manufacturing Directorate, Wright Patterson Air Force Base, OH 45433, USA.

well as in vesicles.[21,22] An advantage of QENS is the large difference in incoherent scattering from hydrogen and its deuterium isotope. Hence selective deuteration is commonly used for the measurement of specific chemical group dynamics. An example is the work of Doxastakis *et al.*[23] where head and tail deuterated DPPC lipids were used in the dehydrated state to understand the mobility of each lipid component. Albeit being in the dry state, this work shows a very clear difference in dynamics and gives insight into the mechanism of the lipid melting transition. In the dry state, head groups are rather immobile and show no signs of a L_β (gel) to L_α (liquid) phase transition. In contrast, the acyl tails relax though *trans–gauche* conformational transitions even in the L_β phase and are ultimately responsible for the phase transition *via* a gradual melting of the heterogeneous hydrophobic domain. In the hydrated state, QENS data have shown similar results, in the gel phase acyl chains are likely only relax through chain-kink diffusion.[10] In more recent work, Wanderlingh *et al.*[16,17] have carefully characterized the dynamics of D_2O hydrated bilayers of DMPC and POPC. Their results revealed three motions occurring in three distinct timescales (between 0.3 and 350 ps): a slow diffusion of the whole lipid within a confined cylinder, conformational relaxations of the lipid chains, and fast uniaxial rotations of the protons around their carbon atoms. When crossing the gel to fluid transition, there is a clear increase in the segmental motion of the terminal part of the lipids plus a change in diffusional dynamics from rattling to confined diffusion.

Using tail deuterated lipids in D_2O, Trapp and co-workers have shown a strong influence of hydration on the head group dynamics, increased mobility is observed as water content is increased.[15] Using fully deuterated lipids with various degrees of water hydration, perturbation to the dynamics of water in lipid headgroups compared to bulk-water has been shown.[6,14] In another study, fully deuterated purple membrane in H_2O or hydrogenated purple membrane in D_2O showed a coupling between membrane dynamics and bacteriorhodopsin but a decoupling with water dynamics at ps–ns time scale and up to 260 K where both membrane and water of hydration go through a dynamical transition.[24] Selective deuteration has also been used to mask DPPC in sterol–lipid mixtures allowing for the observation of jump-diffusion and in-plane rotation of sterol groups. An anisotropy of the in-plane and out-of-plane diffusion of the sterols was also observed.[25,26]

Most natural membranes are a complex mixture of different lipid molecules, each in different states at a given temperature. The chain length and degree saturation of the phospholipids can significantly influence the density, fluidity and phase transition, giving rise to complex phase behaviour. Furthermore, lipids of different types, respond differently to outside factors, for example oxidation, which is of key importance for understanding serious diseases such as cancer, Parkinson's and atherosclerosis.[27,28] Despite its simplicity, understanding the properties of model systems consisting of pure lipid species can provide a basis for understanding how lipid composition ultimately influences membrane dynamics and transport through the membrane. In this paper, we characterize two systems of oriented multilayers, one consisting of dimyrostoyl phosphocholine (DMPC) and the other dioleoylphosphocholine (DOPC) membranes, both at a chosen relative humidity (RH) 75%. We explore the influence of saturation, the double bond, on the lipid dynamics on the nanoscale at temperatures above and below the phase transition. Most QENS studies have been carried out on saturated lipids such as DMPC, DPPC or DMPS, except for the recent studies on POPC.[16,17] The latter mainly concentrated of proposing a very detailed model analysis of motions rather than discussing on the differences between dynamics and lipid structure. To our knowledge only one QENS measurement of DOPC has been performed but in a mixture with DOPS.[29] Here we compare DOPC and DMPC single lipids whose structures are depicted in Fig. 1. Lipid bilayers formed by both of these lipid species exhibit similar headgroup–headgroup spacing, D_{HH}, as shown in Table 1 but their microelastic properties differ to a large degree. We compare both elastic scattering as a function of temperature and the lipid dynamics at fixed temperatures above and below their respective melting transitions using direct geometry and backscattering neutron scattering spectrometers. By transforming the dynamic structure factor, $S(Q,\nu)$ into the time domain, we combined the intermediate scattering function, $I(Q,t)$, from the two instruments using a stretch exponential, to probe dynamic processes over multiple time scales ranging from 10^{-13} to 10^{-9} second. We further analyzed the elastic incoherent structure factor (EISF) for both

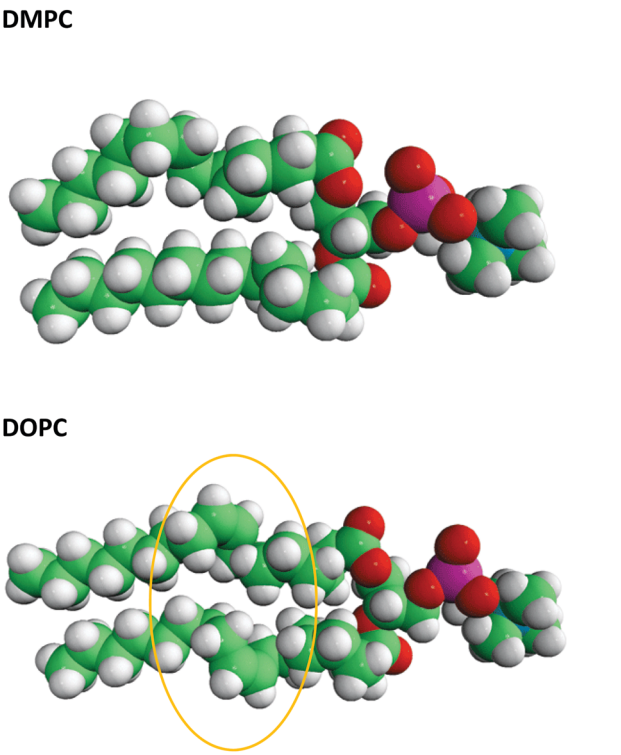

Fig. 1 Chemical structure of DOPC and DMPC. Both lipid monomers form bilayers of approximately the same hydrophobic thickness. While structurally similar DOPC membranes are significantly more fluid and have a lower melting temperature. This difference is due to the unsaturated double bond between carbons in the middle of the lipid tails, which impart a kink in the chain (circled in yellow).

Table 1 Comparison of structural and dynamic properties of DOPC and DMPC lipid bilayers. D_{HH}: mean headgroup to headgroup distance in bilayer, K_A: elastic area stretch modulus, K_C: elastic bending modulus, A_{lipid}: area per lipid, V_{lipid}: volume per lipid

	DOPC	DMPC
D_{HH} (Å)	36.7[b]	35.3[a]
K_A (dyn cm^{-1})	265[c]	234[c]
K_C (10^{-12} erg)	0.80[c]	0.56[c]
A_{lipid} (Å^2)	72.4[b]	60.6[a]
V_{lipid} (nm^3)	1.303[b]	1.101[a]

[a] From ref. 31. [b] From ref. 32. [c] From ref. 33.

systems to gain some insight into the geometry of the dynamics, which fits well to a restricted diffusion model.

The results indicate that the progression of DMPC mobility with increasing temperature occurs over a wider range for DOPC, resulting in a high mobility of the chains already prior to T_m, but only because of its higher T_m. In contrast DOPC just above T_m still has a high fraction of immobile atoms which only relax at temperatures above T_m in the time window of the backscattering spectrometer. If we compare DMPC and DOPC at the same temperature relative to T_m, the emerging picture suggests that the constraint imposed by double bonds in the DOPC chains restrict dynamical motions in both liquid and gel phases compared to DMPC. The very fast dynamic regime, motions of protons on timescales less than a few picoseconds, is fairly similar although DOPC shows slightly lower dynamical amplitude.

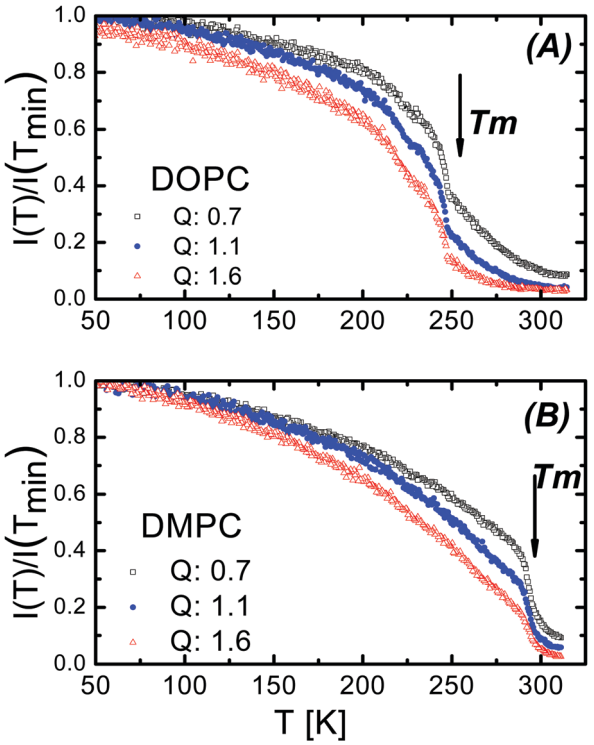

Fig. 2 Elastic intensity scans of (A) DOPC and (B) DMPC lipid bilayers. DOPC lipids show a gradual phase transition at the melting temperature especially at smaller length scales. In contrast, DMPC bilayers undergo a concerted first order phase transition at all length scales probed. Furthermore, DOPC lipids continue to exhibit a large degree of elastic intensity after the T_m, which is gradually lost with increasing temperature.

Results and discussion

Elastic scattering

Changes in the elastic scattering intensity as a function of temperature indicate the activation of anharmonic motions, such as methyl group rotations or diffusional processes. The elastic intensity as a function of temperature and wave vector was measured for the DOPC and DMPC bilayers and is shown in Fig. 2.

For both lipids the gel to liquid phase transition is evident as a discontinuous jump in the elastic intensity as particularly evident at smaller Q values. The observed melting temperatures of DOPC at ~245 K and DMPC at ~295 K are in good agreement with reported values for these systems at 75% RH.[9] For DOPC there appears to be slight indication of a pre-transition starting near 215 K indicating an activation of anharmonic motions below the T_m.

Prior to the melting transitions a significant drop in elastic intensity is observed for both lipid species due to the onset of several dynamic processes. Maybe owing to the higher T_m for DMPC, the data shows that in DMPC the lipid molecules undergo and additional temperature dependent drop in elastic intensity before reaching T_m. Thus, after T_m is crossed, there is very small fraction of protons which have not fully relaxed within the time window of the backscattering spectrometer. In contrast, in DOPC the elastic fraction is rather high as T_m is approached and extra mobility is attained upon changing phase, such that there is a second gradual gain in dynamics as the temperature is increased to room temperature. We emphasize that in both cases, most of the incoherent signal is from the protons in the acyl chains of the lipids. The most likely interpretation is that as the temperature is increased, the hydrophobic chains span increasingly larger volumes, especially the bottom part of the chains, and more protons from the acyl tails that are closer to the head groups are able to move. In the case of DMPC the mobility increase is gradual. For DOPC where the chains have double bonds, a plausible interpretation would be that the gradual increase in dynamics before T_m is due to the bottom half of the chains (consistent with an elastic fraction of about 50% at T_m), involves unlocking of the double bond constraints at T_m, and a further gradual mobility increase with temperature for the whole chain above T_m.

Mean square displacements, $\langle u^2 \rangle$, were calculated from the measured incoherent elastic neutron scattering using the Debye–Waller factor approximation under the Gaussian approximation given by $I(T)/I(T_{min}) = \exp(-Q^2\langle u^2 \rangle/3)$, neglecting translational diffusion. A plot of natural logarithm of the elastic intensity as a function of Q^2 is shown in Fig. 3(A) and (B) for DOPC and DMPC respectively. There is a clear separation of elastic intensities above and below the melting temperature for DMPC compared to DOPC. Below ~200 K the data show a linear behaviour with temperature indicating that dynamics are dominated by vibrational/harmonic motions. At ~200 K the

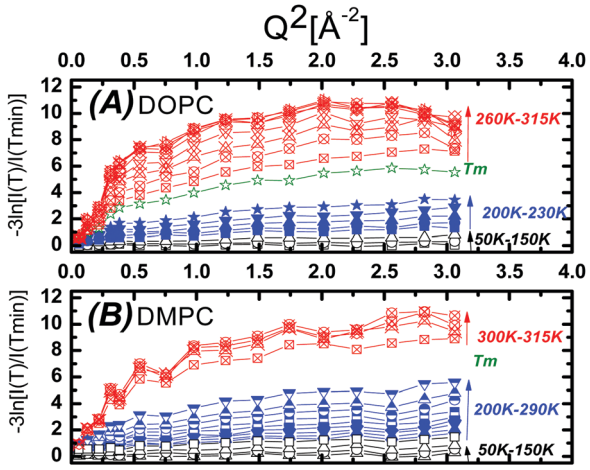

Fig. 3 The slope of the elastic intensity as a function of Q at each temperature was used to calculate the mean square displacement (MSD) of the lipid monomers (see text). Panel (A) and (B) show the elastic intensity for the DMPC and DOPC bilayers respectively. The large gap in the DMPC system is indicative of a cooperative phase transition.

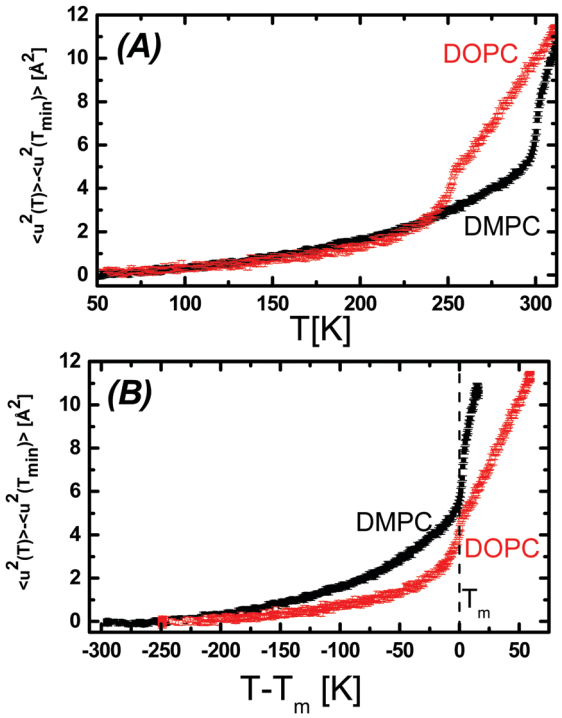

Fig. 4 Mean square displacement for DOPC & DMPC calculated over a reduced Q-range corresponding to distances ~10 to ~25 Å ($0.25 < Q < 0.62$ Å^{-1}) as a function of (A) temperature and (B) temperature relative to the respective T_m of each lipid. Error bars throughout the text represent one standard deviation.

slope slowly becomes non-linear with increasing temperature, consistent with the activation of anharmonic motions. Fig. 4(A) shows the calculated $\langle u^2 \rangle$ as a function of temperature for both lipids from the slope over only the larger distances (lower Q-region corresponding to length scales around 10–25 Å) where the Gaussian approximation holds. As the temperature approaches the T_m of DOPC, $\langle u^2 \rangle$ increases to values much larger than that for DMPC, that is in the gel phase. Above the melting transition of DOPC, $\langle u^2 \rangle$ continues to increase with temperature. In addition, in the temperature range of 140 K to 230 K, the localized modes of DOPC are slightly suppressed compared to DMPC. This might indicate that the double bonds in the acyl chains of DOPC restrict longer length scale motions. Below 140 K harmonic vibrations and methyl group rotations are the dominant dynamical modes for both lipid types.

Furthermore, it is interesting to compare the behaviour of DOPC and DMPC as a function of temperature relative to their respective T_ms, as they differ by only 50 K. Fig. 4(B) shows $\langle u^2 \rangle$ plotted as a function of $(T - T_m)$ for both lipid types. It becomes apparent that the volume explored by DOPC at the onset of localized acyl chain motions, *trans–gauche* conformational transitions or kink-like modes, above 140 K, is more reduced for DOPC, likely due to the double bonds in the acyl chains. Interestingly, close to T_m both lipids are able to explore similar volumes, but above T_m DOPC still is able to explore less volume due to the stiffer chain conformation.

Quasielastic scattering

Macromolecules exhibit complex dynamics that consist of a variety of dynamic and relaxation modes that occur on different time and length scales. QENS is a useful method to probe motions on the 0.5 ps to 5 ns timescale while at the same time monitoring the sensitivity of such motions to length-scale by measuring scattering intensities as a function of Q. The energy resolved spectra of DOPC and DMPC in both gel and liquid phases are presented in Fig. 5. Data are shown from the DCS (timescale < 40 ps) and HFBS (timescale > 200 ps) spectrometers. Lipids in both the gel and liquid phases have significant quasielastic broadening that is indicated by the increased width observed in these samples compared to a pure elastic scattering vanadium standard. This finding indicates that there are relaxation processes in both gel and liquid phase for these lipids. The data are plotted for $Q = 1.05$ Å^{-1} with normalized peak heights. The quasielastic scattering of DMPC is only slightly broader than that observed of DOPC as measured by DCS (Fig. 5A) at both temperatures. For DCS the frequency range of the instrument is most sensitive to motions on the scale of 1 ps. However, the quasielastic scattering measured by HFBS which samples motions over a longer timescale than DCS, shown in Fig. 5B, shows much larger differences between the two lipids. In the gel phase, close to the onset of T_m smaller broadening of the DOPC spectra compared to DMPC (Fig. 5B) indicates that DOPC is not very mobile in the nanosecond timescale, whereas DMPC shows much larger mobility. As the temperature is increased above T_m for DOPC, the broadening increases and becomes larger than that for DMPC in the gel phase, as expected. This is consistent with the elastic scan data where DOPC shows less elastic scattering and larger mean square displacements. At the highest temperature of 315 K, DMPC is the liquid phase, the mobility of DMPC is rather high. In summary, it appears that DOPC and DMPC have similar fast picosecond dynamics and have dramatically different dynamics in the liquid phase when compared at

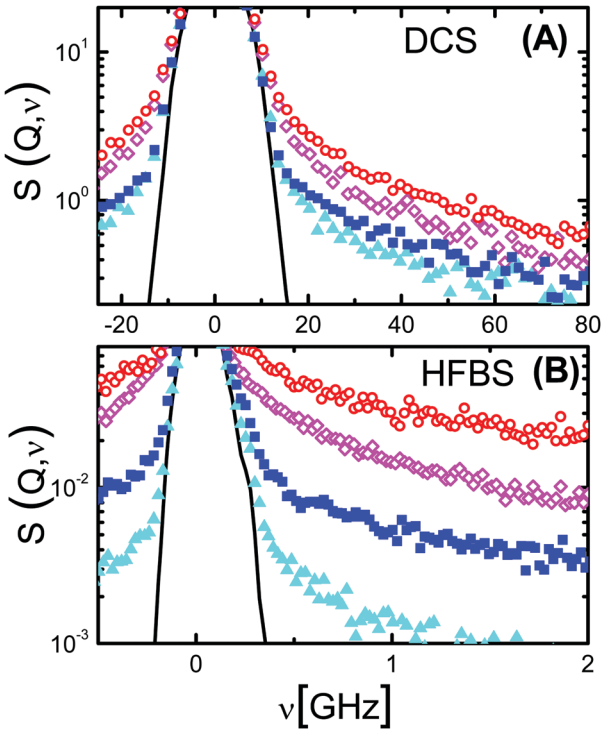

Fig. 5 (A and B) Dynamic structure factor, $S(Q,\nu)$, from time-of-flight disk-chopper and high-flux backscattering spectrometers respectively. Data for DOPC is shown at 245 K (cyan triangles) and 274 K (purple diamonds), while DMPC is shown for 295 K (blue squares) and 315 K (red circles). $S(Q,\nu)$ of vanadium is shown as a solid black line. The data are plotted normalized for peak intensity for Q = 1.05 Å^{-1}.

a similar temperature above their respective T_m (Fig. 4B). At the same $(T - T_m)$ atoms in DMPC are more mobile than atoms in DOPC.

The classical way to analyse QENS data is by fitting the $S(Q,\nu)$ profiles shown in Fig. 5 with a convolution of a delta and Lorentzian functions, where each Lorentzian function is used to describe a type of process which is assumed to be independent of the rest. QENS data on lipid containing systems has been analysed in this way[8,10,14–22,24–26,29] and detailed models developed to describe the geometry of motion in the lipid structures. Lipid molecules, like polymer chains, show very heterogeneous dynamics, owing to the large number of hydrogens in a broad range of environments, which ultimately contribute to the dynamic signal. Each hydrogen atom has a relaxation time that varies significantly from the overall average. Thus, the distribution of relaxation times will be stretched and to analyse the data would require a large number of Lorentzians to describe the system accurately. In the present study, the main objective is to compare the dynamics between DOPC and DMPC, and not to present a detailed descriptive model at the atomic scale. Thus we consider a simplified view of the dynamics, described by an average model which takes into account the breadth of the distribution of relaxation times, namely a stretched exponential function.

The $S(Q,\nu)$ profiles of Fig. 5 are Fourier transformed to obtain the intermediate scattering function, $I(Q,t)$, which can directly be modelled using a stretched exponential of the following form

$$I(Q,t) = (1 - A)\exp\left[-\left(\frac{t}{\tau}\right)^{\beta}\right] + A \qquad (1)$$

where A is the so-called elastic incoherent structure factor (EISF), τ a characteristic relaxation time, and β the exponential coefficient which is a measure of the distribution of relaxation times and/or processes in the system. This form is convenient to combine the experimental data from DCS and HFBS measurements and in this way take advantage of the broad time window accessible (four decades). This method was previously used in the study of anhydrous phospholipids membranes using the same instrumentation[23] and is commonly used to describe relaxation phenomena in soft materials. It should be noted that the ability to fit combined DCS and HFBS data to one stretched exponential does not necessarily imply that the atoms in the system are relaxing in the same way. It is simply a means of providing an average relaxation over all atoms. In some cases and owing to the large energy range covered,[30] it might not be possible to use one single exponential and multiple stretched exponentials are needed. Furthermore, at the short times probed by the DCS spectrometer, caging effects and oscillations of hydrogen atoms around their H-bond directions are likely which are described by models such as that of Liu *et al.*[39] For this work, we concentrate on a comparison of dynamics between lipids at timescales where the cage has relaxed, and so one stretched exponential model is adequate and sufficient.

Plots of $I(Q,t)$ as measured by DCS and HFBS for DOPC and DMPC above and below their respective T_m at three representative Q-values (0.77, 1.05 and 1.61 Å^{-1}) are shown in Fig. 6. Both DOPC and DMPC exhibit qualitatively similar dynamics below their melting temperatures. Additionally, regardless of lipid composition or

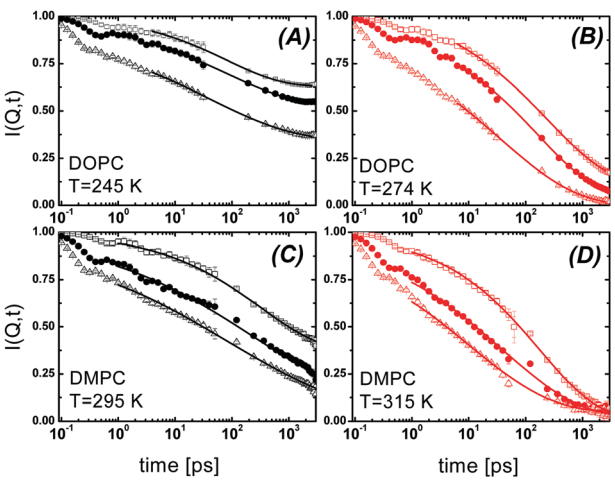

Fig. 6 Relaxation dynamics of DOPC and DMPC. Intermediate scattering functions, $I(Q,t)$, obtained from Fourier transformation of $S(Q,\nu)$ of DOPC (A) and (B) and DMPC (C) and (D) measured by time-of-flight disk chopper and high-flux backscattering spectrometry. Effects of finite instrumental resolution have been removed. Panels (A) and (C) present gel-phase dynamics and panels (B) and (D) present liquid-phase dynamics. $I(Q,t)$ is plotted for various values of momentum transfer, Q. In each panel from top to bottom Q values are 0.77, 1.05, and 1.61 Å^{-1}.

temperature, and as expected, there is evidence of caging that occurs before approximately 2–3 ps. In this paper we focus our attention on the relaxational dynamics and thus fit the stretched exponential function to data at $t > 3$ ps. Exemplary fits are shown in Fig. 6.

The KWW characteristic relaxation times extracted from the fits (Table S1, ESI†) for DOPC at 274 K (in the liquid phase) are slightly larger than at 245 K. For DOPC at 274 K KWW relaxation times vary between 260 ps to 31 ps, and at 245 K between 84 ps and 30 ps, depending on the Q-value considered. DOPC on average is dynamically slower in the liquid phase than in the gel phase which seems counter intuitive. Even though the protons are able to explore more space, the dynamical processes taking place are slower and in addition due to the double bond constraints a different population of protons may be contributing to the average. At the largest Q-values which correspond to small distances probed, the dynamics in both phases is similar, owing to averaging over fast and temperature independent motions. DMPC behaves as expected, with faster dynamics in the liquid phase, the KWW characteristic relaxation times at 315 K vary between around 49 ps to 5 ps, and at 293 K between 74 ps and 8 ps, depending on the Q-value considered. The behaviour is consistent when average relaxation times are considered (Fig. S4, ESI†). For DMPC where motions are not constrained by double bonds in the acyl tails, all protons likely contribute to the average motions at all temperatures. The Q dependence of the relaxation times is plotted in Fig. S4A (ESI†) – both lipids show a Q^{-2} dependence typical of heterogeneous dynamics as seen in polymer systems. The temperature dependence of the average relaxation times is plotted in Fig. S4b (ESI†) at the average Q. Despite having only two temperature points it is clear that DMPC dynamics shows a somewhat stronger temperature dependence. Further analysis of the dynamical data in the frequency domain using a Cole–Cole function is shown in Fig. S3 (ESI†).

The stretching exponent (Table S1 and Fig. S5, ESI†) obtained from the fits is similar for both lipids showing no temperature dependence, however they are strongly Q dependent. At $Q < 1$ Å^{-1} (corresponding to motions >6 Å) there is a monotonic decrease of β from ~ 0.5 (which is typical for amorphous polymers) to around 0.3, where it reaches a plateau for $Q > 1$ Å^{-1} (corresponding to motions <6 Å). At a local length scale ($Q > 1$ Å^{-1}) we are probing the heterogeneity in the proton mobility, whereas at the larger length scales ($Q < 1$ Å^{-1}) one averages dynamics over many protons performing different motions and thus represents an average, as observed for linear polymer chains.

The relaxation behaviour for the two lipids is clearly different and the experimental data obtained through quasielastic neutron scattering is sensitive to different dynamical processes between the gel and fluid phase systems. In the gel phase motions are much more restricted, possibly due to highly localized, fast, rattling motions. Long-range spatial motions are out of the time window for the HFBS instrument in the gel phase. However, once the lipid system is in the fluid phase some long-range motions are brought into the resolution of the instrument and can be observed. These motions however may actually increase the relaxation times, as is the case for DOPC, but would result in a lower EISF. Such motions may include active transitions of torsion angles, lipid rotation, and perhaps even localized lateral diffusion.

We concentrate on the residual elastic intensity as a function of Q that can be used to obtain atomic insight into the observed dynamics from QENS data, and ties in with the elastic scattering measurements. We choose to use an analytical expression for the EISF which describes the dynamics along the carbon backbone of the lipid monomers as diffusion in a sum of spheres of increasing radius. This description was used originally by Carpentier *et al.*[34] and has been used successfully for lyophilized lipid chains[23] and surfactant micelles.[35] The model is represented by the following analytical expression.

$$A(Q) = \frac{1}{N}\sum_{n=1}^{N}\left[\frac{3j_i(QR_n)}{QR_n}\right]^2 \quad (2)$$

where

$$R_n = \frac{n}{N}[R_N - R_2] + R_2 \quad (3)$$

and R is the spherical radius, $A(Q)$ the EISF and $j_i(QR)$ the first order spherical Bessel function.

Our model anchors motion relative to the second carbon atom of each chain and neglects motion of the hydrogens in the head group, analogous to the methods used to interpret the dynamics of saturated DPPC lipid systems.[8,23] Qualitatively, using eqn (2) and (3) the EISF is fit by a collection of spheres with a linearly increasing spherical size distribution from carbon 2 to the terminal methyl groups on each lipid monomer chain. The quality of the fit using $N = 14$ spheres is shown in Fig. 7 as well as a fit considering just two spheres. The quality of

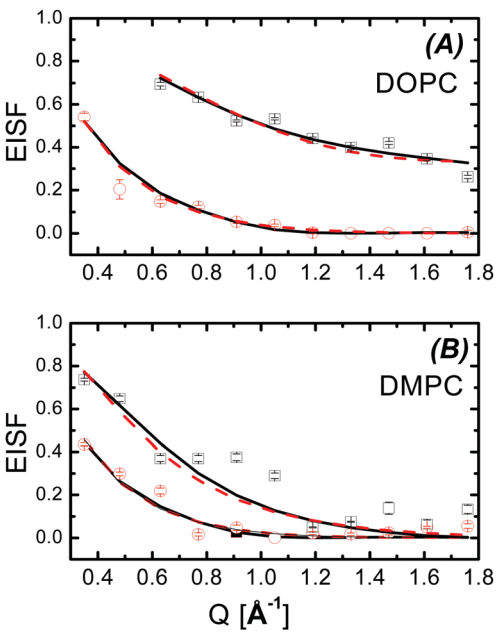

Fig. 7 Elastic incoherent structure factor (EISF) as a function of Q. The EISF provides insight into the geometry of motion in the individual lipid chains. Panel (A) shows EISF data for the DOPC bilayers and panel (B) for DMPC, in both the gel and fluid state. Lipid chain motions were modelled using a linear distribution of spheres representing carbon positions along the chain. There results of fitting this model are shown using solid where $N = 2$, and dashed lines where $N = 14$.

Table 2 Parameters of fit of the EISF to a model of diffusion in a sum of spheres distributed linearly along the lipid tails (N = 2 or N = 14)

	N = 2		N = 14	
	R_{min} (Å)	R_{max} (Å)	R_{min} (Å)	R_{max} (Å)
DOPC 245 K	0.82 ± 0.01	2.90 ± 0.2	0 ± 0	2.48 ± 0.01
DOPC 274 K	3.42 ± 0.04	6.75 ± 0.28	2.48 ± 0.07	8.36 ± 0.30
DMPC 293 K	2.37 ± 0.01	3.97 ± 0.06	1.18 ± 0.02	5.38 ± 0.08
DMPC 313 K	3.77 ± 0.06	7.73 ± 0.20	2.73 ± 0.01	9.11 ± 0.02
DPPC 350 K[a]			0.79 ± 0.03	5.85 ± 0.16
DPPC 370 K[a]			0.86 ± 0.08	6.19 ± 0.45
DMPC 303 K[b]	0	3.2		
POPC 298 K[b]	0	4.2		
DMPC 303 K[c]	$2R$ = 8.50	L = 3.73		
POPC 298 K[c]	$2R$ = 10.2	L = 3.50		

[a] Lyophilised (T_m ~ 350 K), model with N = 16.[23] [b] Fully hydrated, sphere model for intermediate dynamics.[17] [c] Fully hydrated, restricted diffusion in a cylinder of length L and diameter $2R$.[17]

the fits is equivalent – the lipids can be approximated by two spheres of varying radii corresponding to top part of the chain and bottom part of the chain. Due to the low-resolution "coarseness" of sphere models we hesitate to unequivocally associate the spheres as near head-group and acyl-chain specifically, as sphere diameter may invalidate such a definition. For both DOPC and DMPC the gel phase has more residual intensity than the corresponding liquid phases that is consistent with reduced atomic motion of lipid atoms below the T_m. However, in DOPC the extent of residual intensity around T_m is significantly higher, consistent with a reduced mobility observed in the elastic data. Table 2 shows the values obtained for R_{min} and R_{max} from the fits. At the lowest temperature, the top part of the acyl chains in DOPC is almost immobile (if we consider a two-sphere model R_{min} is <1 Å, and for N = 14 model R_{min} is almost zero) while the bottom part explores a volume with the radius between 2.5 and 3 Å. The mobility of the bottom part of DOPC remains less than that of the extent of motion of DMPC at the low temperature (N = 2 model: between 2.4 and 4 Å and in N = 14 model between 1.2 and 5.4 Å). In the liquid phase, DOPC is able to explore a larger volume and the top part shows a distinct change. For the N = 2 model, $3.2 < R$ (Å) < 6.8 and for the N = 14 model, $2.5 < R$ (Å) < 8.4. For DMPC there is approximately a two-fold increase in the sphere radius after crossing T_m, but no separate behaviour is observed between top and bottom of the tails. For the N = 2 model, $3.8 < R$ (Å) < 7.7 and for the N = 14 model, $2.7 < R$ (Å) < 9.1. Once in the liquid phase, the amplitude of motion for both lipids is similar but DOPC is still not able to explore as much volume as DMPC. Comparing the values obtained for a similar lipid DPPC albeit in lyophilized state is also shown in Table 2. The values obtained of R_{min} and R_{max} are in the same range as those of DPPC, albeit in lyophilized state (Table 2), in the gel phase. The DPPC data are expected to be less mobile since they only contain 2 wt% residual water content compared with lipids in the current study (75% RH). Wanderlingh *et al.*,[17] proposed two different types of motions in the timescales considered here, for DMPC and POPC albeit at a higher hydration (28 D_2O molecules per lipid). Their results show that near ~300 K both the *trans–gauche* conformational transitions and the slower whole lipid monomer motions are slightly larger for POPC than DMPC, but this is most likely due to the higher temperature above T_m of POPC as compared with DMPC.

The local diffusion in a sphere model captures the basic property of increasing diffusion as a function of going from the gel to fluid phase. However, determining the number of spheres, or scattering centers, required to model the EISF data and making physical sense of the very low R_{min} when using more than three spheres is a difficult problem highlighting a fundamental limit of using such models. Atomistic modelling of lipid membranes is one such method that can be used to help in the understanding of factors leading to the large dynamical differences and their connection to macroscopic properties.

Conclusion

Neutron scattering has proven to be a useful tool to study the structure and dynamics of a soft condensed matter in amorphous and fluid phase systems. Through the transformation of dynamical structure factors determined by neutron experiments one can obtain time domain data across a variety of length scales that probe relevant molecular dimensions. This type of time dependent data has led to a physical understanding of molecular motions through analytical models as those discussed herein. However, the chemical and structural diversity of biological systems provide special challenges in both data collection and interpretation.

One approach is to simplify molecular systems into component species to provide a baseline for the dynamical properties inherent in each part. In this study, we compared the dynamics of two oriented multi-lamellar bilayer systems consisting of different lipids species. DMPC represented a model of a fully saturated acyl-chain lipid species while DOPC was used to represent an unsaturated chain counterpart. Despite similar membrane thicknesses, DOPC exhibits significantly lower bending and compressibility moduli compared with DMPC. We found that the inherent differences in material properties may be reflected in the different temperature dependent structural relaxation properties of the lipid chains. However, caging effects found at short, picosecond time scales were almost identical between lipid types over a range of length scales. Perhaps dynamical regimes within soft condensed materials exist that may not necessarily couple into longer processes.

Combined experimental and molecular simulations methods can further probe the coupling of different dynamical relaxation times by providing atomistic detail with regard to molecular motion. Ultimately the goal is to predict the dynamic responsiveness of mixed lipid membrane systems from their individual components. This behaviour is unlikely to be purely additive due to factors such as non-ideal lipid mixing and lateral heterogeneity. Selective deuteration of each species provides a mechanism to compare the difference of lipids species in mixed or pure lipid environments and is only possible by neutron scattering.

Experimental

Sample preparation

1,2-Dimyrostoyl-*sn-glycero*-3-phosphocholine (DMPC) and 1,2-dioleoyl-*sn-glycero*-3-phosphocholine (DOPC) were obtained from Avanti Lipids (Alabaster, AL).‖ Sodium chloride (NaCl) and methanol were obtained from Sigma-Aldrich (St. Louis, MO) and D_2O from Cambridge Isotopes (Andover, MD). Polished 0.5 mm thick Si(1,0,0) wafers were obtained from EL-CAT (Waldwick, NJ).

For each lipid preparation, fifteen 10 mm × 35 mm slides were cut from the Si wafers. Lipids were dissolved in methanol at 400 mg ml^{-1}. 0.625 ml of solution was plated on the slides equally resulting in approximately 250 mg of total lipid per condition studied. The lipid samples were dried under vacuum overnight and then re-hydrated in D_2O vapor using saturated NaCl salt solutions. Both samples were sealed under helium to ensure proper heat transfer across the sample. The sealed sample chamber was given several hours to equilibrate to 75% RH.

Neutron transmission was measured using the NG3 small angle neutron scattering, SANS, instrument at the National Institute of Standards and Technology Center for Neutron Research in Gaithersburg, MD. Both samples had ~92% transmission. Furthermore, analysis of SANS data confirmed that the lipid membranes formed oriented planar bilayers with low mosaic spread (~0.6°). See Fig. S1 (ESI†) for a schematic of sample orientation and geometry.

Incoherent neutron scattering

Quasielastic neutron scattering experiments were performed using the time-of-flight disk chopper spectrometer[36] and the high-flux backscattering spectrometer[37,38] at the National Institute of Standards and Technology Center for Neutron Research in Gaithersburg, MD. Measured neutron intensities were analyzed using the DAVE software.[40] Intensities were corrected for detector efficiency by comparison with a vanadium standard and for scattering from empty sample cans to enable the calculation of a time-independent background. All quasielastic scans provide the dynamic structure factor, $S(Q,\nu)$, within the time and spatial resolution of the instruments. The intermediate scattering function, $I(Q,t)$, was obtained from using methods previously described[41] with deconvolution with the appropriate resolution function for the instrument used. Combined, these instruments are capable of measuring the incoherent dynamics from 0.5 ps to 5 ns over a spatial range of 4 to 25 Å. In all figures, uncertainty is represented as ±1 standard deviation and is denoted by error bars in cases where the uncertainty is larger than the symbols representing the measured data. The lipids are fully hydrogenated and at 75% RH. in D_2O most of the scattering is incoherent from the protons throughout the lipid molecules. For both lipid types the incoherent scattering is around 90% of the total scattering signal. Since most of the protons are located in the acyl chains, the measured signal in the QENS data will be representative of the dynamics of the acyl chains (between 80–85% of the lipid incoherent signal).

Time-of-flight disk chopper spectrometer

The time-of-flight disk chopper spectrometer (DCS) was used with an incident wavelength of 6.4 Å providing an energy resolution of ≈54 μeV measured at full width at half-maximum determined by calibration with a vanadium standard. Data were measured at 295 K and 315 K for DMPC and 245 K and 274 K for DOPC. Vanadium standard was used as instrumental resolution.

High-flux backscattering spectrometer

The high-flux backscattering spectrometer (HFBS) used an incident neutron wavelength that was varied by Doppler shifting, at the value of 6.271 Å. Scattered neutrons were passed through Si(1,1,1) Bragg analyzer crystals such that detectors collected neutrons with a final energy of 2.08 meV. A dynamic range of ±17 μeV was used that provided an energy resolution of 0.86 μeV that was confirmed by measuring a vanadium standard. In the present setup, $S(Q,\nu)$, was measured at 295 K and 315 K for DMPC and 245 K and 274 K for DOPC. A vanadium standard was used as the instrumental resolution. In addition, elastic scans of DOPC and DMPC were separately carried out using HFBS with the Doppler drive at rest to collect the elastic intensity as a function of temperature from 10 K to 315 K at a heating rate of 1 K per minute. Scattering data were collected for wave vectors from 0.25 $Å^{-1}$ to 1.76 $Å^{-1}$ to correspond to the length scales measured by DCS.

Conflicts of interest

There are no conflicts to declare.

Acknowledgements

This work utilized facilities supported in party by the National Science Foundation under agreement no. DMR-0944772. H. N. acknowledges support from the NIH R01-GM101647-02. S. K. acknowledges funding from the National Research Council. Access to the HFBS was provided by the Center for High Resolution Neutron Scattering, a partnership between the National Institute of Standards and Technology and the National Science Foundation under Agreement No. DMR-1508249.

Notes and references

1 S. J. Singer and G. L. Nicolson, *Science*, 1972, **175**, 720–731.
2 K. Gawrisch and O. Soubias, *Chem. Phys. Lipids*, 2008, **153**, 64–75.
3 C. W. Mullineaux and H. Kirchhoff, *Methods Mol. Biol.*, 2007, **400**, 267–275.
4 S. Vehring, L. Pakkiri, A. Schroer, N. Alder-Baerens, A. Herrmann, A. K. Menon and T. Pomorski, *Eukaryotic Cell*, 2007, **6**, 1625–1634.

‖ Certain commercial equipment, instruments, materials, suppliers, or software are identified in this paper to foster understanding. Such identification does not imply recommendation or endorsement by the National Institute of Standards and Technology, nor does it imply that the materials or equipment identified are necessarily the best available for the purpose.

5 A. A. Nevzorov and M. F. Brown, *J. Chem. Phys.*, 1997, **107**, 10288–10310.
6 S. Konig, E. Sackmann, D. Richter, R. Zorn, C. Carlile and T. M. Bayerl, *J. Chem. Phys.*, 1994, **100**, 3307–3316.
7 T. Takeda, Y. Kawabata, H. Seto, S. Komura, S. K. Ghosh, M. Nagao and D. Okuhara, *J. Phys. Chem. Solids*, 1999, **60**, 1375–1377.
8 S. Konig, W. Pfeiffer, T. Bayerl, D. Richter and E. Sackman, *J. Phys. II*, 1992, **2**, 1589–1615.
9 W. Pfeiffer, T. Henkel, E. Sackmann, W. Knoll and D. Richter, *Europhys. Lett.*, 1989, **8**, 201–206.
10 S. Konig, T. M. Bayerl, G. Coddens, D. Richter and E. Sackmann, *Biophys. J.*, 1995, **68**, 1871–1880.
11 L. R. Arriaga, I. Lopez-Montero, F. Monroy, G. Orts-Gil, B. Farago and T. Hellweg, *Biophys. J.*, 2009, **96**, 3629–3637.
12 B. Klosgen, C. Reichle, S. Kohlsmann and K. D. Kramer, *Biophys. J.*, 1996, **71**, 3251–3260.
13 A. Blume, *Curr. Opin. Colloid Interface Sci.*, 1996, **1**, 64–77.
14 J. Swenson, F. Kargl, P. Berntsen and C. Svanberg, *J. Chem. Phys.*, 2008, **129**, 045101.
15 M. Trapp, T. Gutberlet, F. Juranyi, T. Unruh, B. Deme, M. Tehei and J. Peters, *J. Chem. Phys.*, 2010, **133**, 164505.
16 U. Wanderlingh, C. Branca, C. Crupi, V. C. Nibali, G. La Rosa, S. Rifici, J. Ollivier and G. D'Angelo, *J. Chem.*, 2017, **2017**, 3654237.
17 U. Wanderlingh, G. D'Angelo, C. Branca, V. C. Nibali, A. Trimarchi, S. Rifici, D. Finocchiaro, C. Crupi, J. Ollivier and H. D. Middendorf, *J. Chem. Phys.*, 2014, **140**, 174901.
18 L. Toppozini, F. Roosen-Runge, R. I. Bewley, R. M. Dalgliesh, T. Perring, T. Seydel, H. R. Glyde, V. García Sakai and M. C. Rheinstadter, *Soft Matter*, 2015, **11**, 8354–8371.
19 M. A. Barrett, M. Trapp, W. Lohstroh, T. Seydel, J. Ollivier, M. Ballauff, N. A. Dencher and T. Hauß, *Soft Matter*, 2016, **12**, 1444–1451.
20 S. Busch, C. Smuda, L. C. Pardo and T. Unruh, *J. Am. Chem. Soc.*, 2010, **132**, 3232–3233.
21 V. K. Sharma, E. Mamontov, M. Tyagi, S. Qian, D. K. Rai and V. S. Urban, *J. Phys. Chem. Lett.*, 2016, **7**, 2394–2401.
22 V. K. Sharma, E. Mamontov, D. B. Anunciado, H. O'Neill and V. S. Urban, *J. Phys. Chem. B*, 2015, **119**, 4460–4470.
23 M. Doxastakis, V. G. Sakai, S. Ohtake, J. K. Maranas and J. J. de Pablo, *Biophys. J.*, 2007, **92**, 147–161.
24 K. Wood, M. Plazanet, F. Gabel, B. Kessler, D. Oesterhelt, D. J. Tobias, G. Zaccaï and M. Weik, *Proc. Natl. Acad. Sci. U. S. A.*, 2007, **104**, 18049–18054.
25 E. Endress, H. Heller, H. Casalta, M. F. Brown and T. M. Bayerl, *Biochemistry*, 2002, **41**, 13078–13086.
26 C. Gliss, O. Randel, H. Casalta, E. Sackmann, R. Zorn and T. Bayerl, *Biophys. J.*, 1999, **77**, 331–340.
27 R. A. Roberts, D. L. Laskin, C. V. Smith, F. M. Robertson, E. M. G. Allen, J. A. Doorn and W. Slikkerk, *Toxicol. Sci*, 2009, **112**, 4–16.
28 A. Reis and C. M. Spickett, *Biochim. Biophys. Acta, Biomembr.*, 2012, **1818**, 2374–2387.
29 W. Knoll, F. Natali, J. Peters, R. Nanekar, C. Wang and P. Kursula, *Spectrosc. Int. J.*, 2010, **24**, 585–592.
30 R. E. Lechner, *Physica B*, 2001, **301**, 83–93.
31 N. Kucerka, Y. F. Liu, N. J. Chu, H. I. Petrache, S. T. Tristram-Nagle and J. F. Nagle, *Biophys. J.*, 2005, **88**, 2626–2637.
32 J. Pan, S. Tristram-Nagle, N. Kucerka and J. F. Nagle, *Biophys. J.*, 2008, **94**, 117–124.
33 W. Rawicz, K. C. Olbrich, T. McIntosh, D. Needham and E. Evans, *Biophys. J.*, 2000, **79**, 328–339.
34 L. Carpentier, M. Bee, A. M. Giroudgodquin, P. Maldivi and J. C. Marchon, *Mol. Phys.*, 1989, **68**, 1367–1378.
35 V. K. Sharma, S. Mitra, G. Verma, P. A. Hassan, V. G. Sakai and R. Mukhopadhyay, *J. Phys. Chem. B*, 2010, **114**, 17049–17056.
36 J. R. D. Copley and J. C. Cook, *Chem. Phys.*, 2003, **292**, 477–485.
37 R. M. Dimeo, Z. Chowdhuri, A. Meyer, P. M. Gehring and D. A. Neumann, *Appl. Phys. A: Mater. Sci. Process.*, 2002, **74**, S311–S313.
38 P. M. Gehring and D. A. Neumann, *Physica B*, 1997, **241-243**, 64–70.
39 L. Liu, A. Faraone and S. H. Chen, *Phys. Rev. E: Stat., Nonlinear, Soft Matter Phys.*, 2002, **65**, 041506.
40 R. T. Azuah, L. R. Kneller, Y. M. Qiu, P. L. W. Tregenna-Piggott, C. M. Brown, J. R. D. Copley and R. M. Dimeo, *J. Res. Natl. Inst. Stand. Technol.*, 2009, **114**, 341–358.
41 V. G. Sakai, C. X. Chen, J. K. Maranas and Z. Chowdhuri, *Macromolecules*, 2004, **37**, 9975–9983.